

NJC

Accepted Manuscript



This article can be cited before page numbers have been issued, to do this please use: B. Zhang, Y. Xiao, H. Fang, H. Gao, F. Wang and X. Cheng, *New J. Chem.*, 2018, DOI: 10.1039/C8NJ02814A.



This is an Accepted Manuscript, which has been through the Royal Society of Chemistry peer review process and has been accepted for publication.

Accepted Manuscripts are published online shortly after acceptance, before technical editing, formatting and proof reading. Using this free service, authors can make their results available to the community, in citable form, before we publish the edited article. We will replace this Accepted Manuscript with the edited and formatted Advance Article as soon as it is available.

You can find more information about Accepted Manuscripts in the [author guidelines](#).

Please note that technical editing may introduce minor changes to the text and/or graphics, which may alter content. The journal's standard [Terms & Conditions](#) and the ethical guidelines, outlined in our [author and reviewer resource centre](#), still apply. In no event shall the Royal Society of Chemistry be held responsible for any errors or omissions in this Accepted Manuscript or any consequences arising from the use of any information it contains.

Mesogenic D-A fluorophores based on cyanovinyl and benzothiadiazole

Bei Zhang,^{‡[a]} Yulong Xiao,^{‡[a]} Haipeng Fang,^[a] Hongfei Gao,^[a] Fuke Wang,^{*[b]}
Xiaohong Cheng^{*[a]}

[a] Key Laboratory of Medicinal Chemistry for Natural Resources, Chemistry Department,
Yunnan University
Kunming,
Yunnan 650091,
P. R. China
Fax: (+86) 871 65032905
E-mail: xhcheng@ynu.edu.cn

[b] Department of Sports Medicine, First Affiliated Hospital of Kunming Medical University
E-mail: wfk.04@126.com

‡Both authors contributed equally to this work

Abstract: A series of donor-acceptor fluorophores containing biscyanovinyl dithienebenzothiadiazole central unit with 4-alkoxyphenyl groups at both sides were synthesized. These compounds can display smectic C and hexagonal columnar mesophases in their bulk states, and aggregate into organogel as well as cubic or needle crystals in organic solvents. These cubic or needle crystals exhibit optical waveguide behavior. Additionally, these compounds can exhibit broad absorption up to 625 nm with a narrow band gap of 1.79 eV. The fluorescence emission of these compounds in CHCl₃ can be quenched upon addition of C₇₀. Further these compounds can detect Cu²⁺ among a series of cations.

1. Introduction

π -Conjugated polymers and small organic molecules have attracted widespread attention due to their potential applications in photoelectronic devices. However defects in polymeric backbone can lead to irreproducible performance and unstable device efficiency. π -Conjugated small organic molecule can be obtained with high purity and synthesized with controllable molecular weights. The well defined characteristics of conjugated small molecules can further aggregate into ordered supramolecular structure, which facilitates the optimal performance of molecular devices.^{1,2}

Cyano group is highly polarisable with a large permanent dipole moment. It has been used to construct mesogens because it can cause strong dipole-dipole interactions.³ The introduction of cyano group onto the scaffold of π -conjugated oligomer or polymer can largely lower the LUMO level of the molecules.⁴ α -Cyanostilbene derivatives have developed as light-active luminescent molecules, with aggregation-induced enhanced emission (AIEE) effect for various applications.⁵

As a strong electron acceptor unit, benzothiadiazole (BTD) have been used to tune the HOMO and LUMO energy levels of low band gap fluorophores.^{6,7} BTD-based fluorophores showed great

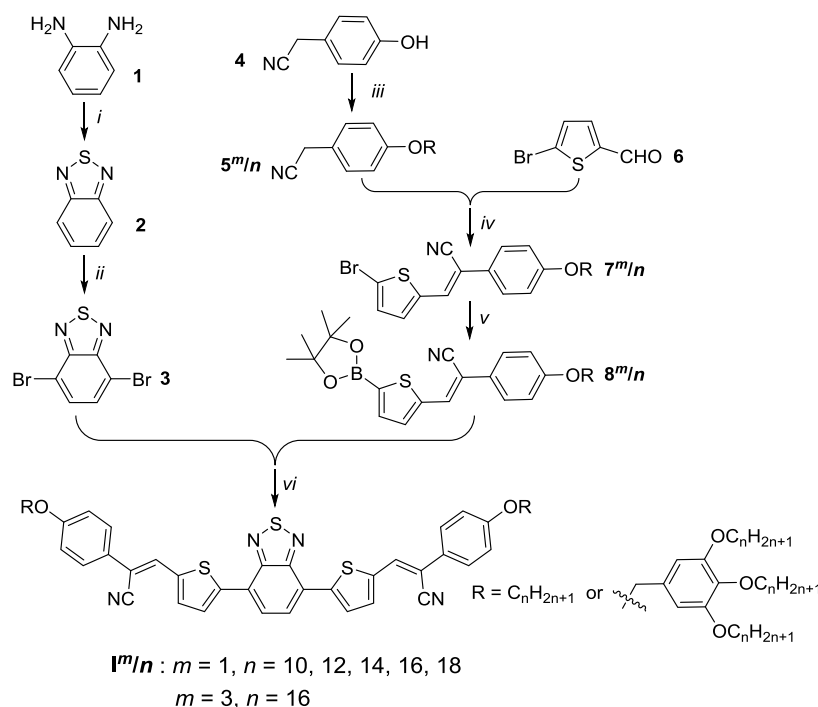
potentials in light emitting diodes,⁸ chemosensors,⁹ solar cells,¹⁰ light-harvesting, and many others.¹¹

Till now, only a few derivatives consisting of BTD and α -cyanostilbene were reported, the overall power conversion efficiencies (PCEs) of the photovoltaic devices based on such derivatives are between 0.1-5.6%.¹² So far as we know, there is only one report about the liquid crystalline properties of BTD α -cyanostilbene derivatives, and only smectic phases were roughly described.¹³ It is commonly considered that mesomorphism would be favorable for better molecular packing, and helpful for good photovoltaic performance.¹⁴ Therefore herein we have designed and synthesized a series of mesogenic D-A fluorophores which contain biscyanovinyl dithienebenzothiadiazole central unit with 4-alkoxyl phenyl groups at both sides. The main goal of this study is as follows: Firstly to study the mesomorphism behaviors of these compounds and establish the relationship between the molecular structure and mesophase properties. Secondly to study the photophysical properties of these compounds as well as their potentials as functional molecular devices.

2. Results and discussion

2.1. Synthesis

Together six compounds were synthesized, including five dicatenars \mathbf{I}^1/n ($n = 10-18$) and one hexacatenar $\mathbf{I}^3/16$. These target compounds \mathbf{I}^m/n (the superscript m and the number n stand for the number and the length of the terminal alkyl chains respectively) were synthesized *via* Knoevenagel and Suzuki reactions as key steps (Scheme 1). Firstly, 4-hydroxybenzyl cyanide **4** was etherified with appropriate halide. Knoevenagel reactions between 5-bromothiophene-2-carbaldehyde **6** and phenylacetonitrile $\mathbf{5}^m/n$ gave compounds $\mathbf{7}^m/n$. By borylation with bis(pinacolato)diborane, $\mathbf{7}^m/n$ were changed to compounds $\mathbf{8}^m/n$. Suzuki reaction between compounds $\mathbf{8}^m/n$ and 4,7-dibromobenzothiadiazole **3**⁹ gave the final products which were purified by column chromatography. More details of procedures and corresponding analysis data were summarized in the Supporting Information (SI).



Scheme 1 Synthetic route of compounds \mathbf{I}^m/n : *Reagents and conditions*: i) SOCl_2 , Et_3N , CH_2Cl_2 , 40°C , 7 h; ii) Br_2 , HBr , 90°C , 12 h; iii) DMF , K_2CO_3 , RBr ($\text{R} = \text{C}_n\text{H}_{2n+1}$) or 5-(chloromethyl)-1,2,3-tris(hexadecyloxy)benzene,¹⁵ 90°C , 5 h; iv) EtOH , MeONa , RT, 1 h; v) Toluene, AcOK , $\text{Pd}(\text{PPh}_3)_2\text{Cl}_2$, PPh_3 , bis(pinacolato)diboron, 120°C , 24 h; vi) Toluene, Na_2CO_3 , H_2O , EtOH , $\text{Pd}(\text{PPh}_3)_4$, 110°C , 36 h.

2.2. Mesomorphic properties

The mesomorphic properties of compounds \mathbf{I}^m/n were investigated by polarized optical microscopy (POM, Fig. 1a and Fig. S1), differential scanning calorimetry (DSC, Fig. S2) and X-ray diffraction (XRD, Fig. 1b, Fig. 2a and Fig. S3). The mesomorphic properties of compounds \mathbf{I}^m/n were collected in Table 1. More detailed data were listed in Tables S1-S6.

Table 1 Thermotropic LC properties and X-ray data of compounds \mathbf{I}^m/n .^a

Comp.	m	n	$T/^\circ\text{C}$ [$\Delta\text{H}/\text{kJ mol}^{-1}$]	d/nm ($T/^\circ\text{C}$)	a/nm ($T/^\circ\text{C}$)	μ
$\mathbf{I}^1/10$	1	10	Cr_1 142.1 [1.38] Cr_2 164.7 [13.10] Cr_3 171.4	3.90 (200)	/	/
			[11.10] SmC 258.8 [2.25] Iso			
$\mathbf{I}^1/12$	1	12	Cr_1 135.2 [18.36] Cr_2 143.6 [18.33] Cr_3 169.8	4.19 (260)	/	/
			[21.32] SmC 263.1 [4.65] Iso			
$\mathbf{I}^1/14$	1	14	Cr_1 133.4 [5.25] Cr_2 147.7 [23.60] Cr_3 160.6	4.34 (247)	/	/
			[26.40] SmC 253.6 [3.50] Iso			
$\mathbf{I}^1/16$	1	16	Cr_1 129.3 [8.88] Cr_2 140.7 [4.06] Cr_3 156.1	4.58 (180)	/	/
			[7.28] SmC 247.9 [1.22] Iso			
$\mathbf{I}^1/18$	1	18	Cr_1 131.4 [17.50] Cr_2 141.9 [11.60] Cr_3 150.5	4.74 (200)	/	/
			[18.60] SmC 234.3 [3.02] Iso			
$\mathbf{I}^3/16$	3	16	Cr 39.3 Col_{hex} 142 ^b Iso	/	5.44 (110)	3.1

^a Transition temperatures ($^\circ\text{C}$) and associated enthalpy values (kJ mol^{-1}), give in brackets were determined by DSC on the second heating scan, at a rate of 3 K min^{-1} . Cr = crystal; SmC = smectic C phase; Col_{hex} = hexagonal

columnar phase; Iso = isotropic liquid; d = layer spacing determined by XRD; a = lattice parameter determined by XRD; μ = number of molecules in a slice of a column in the Col_{hex} phases (with assumed height of 0.45 nm). For Col_{hex} phase: $\mu = (a^2/2)\sqrt{3}h(N_A/M)\rho$, N_A = Avogadro constant, M = molecular mass, assuming a density of $\rho = 1$ g/cm³.^b Transition temperature was determined by POM.

2.2.1. Smectic C phase

All compounds were enantiotropic LCs. For the dicatenar compounds **I¹/*n*** ($n = 10-18$), upon elongation of the terminal alkyl chain length, led to decreasing of both the melting and clearing temperatures (Table 1).

Polarized optical schlieren textures (Fig. 1a and Fig. S1a-d) suggested that all dicatenar compounds self-assembled into SmC phase.¹⁶ The small-angle X-ray scattering (SAXS) patterns of these smectic phases (Fig. 1b and Fig. S3) showed two reflection peaks in the small angle region with a ratio of $d_{001}/d_{002} \approx 2$, confirming the smectic organization.³ The layer spacing of representative compound **I¹/**14**** is about $d = 4.34$ nm at 247 °C (Table S3), which is shorter than the calculated molecular length ($L_{\text{max}} = 5.82$ nm),¹⁷ indicating that a monolayer SmC phase. The tilt angle was calculated to be $\theta \approx 42^\circ$ (based on the relationship $\cos\theta = d/L_{\text{max}}$) from the layer normal (Fig. 1c). These diameters are also consistent with the sizes of the cores (green) and alkyl chains (white) in the molecular dynamics (MD) annealed model¹⁸ in Fig. 1d.

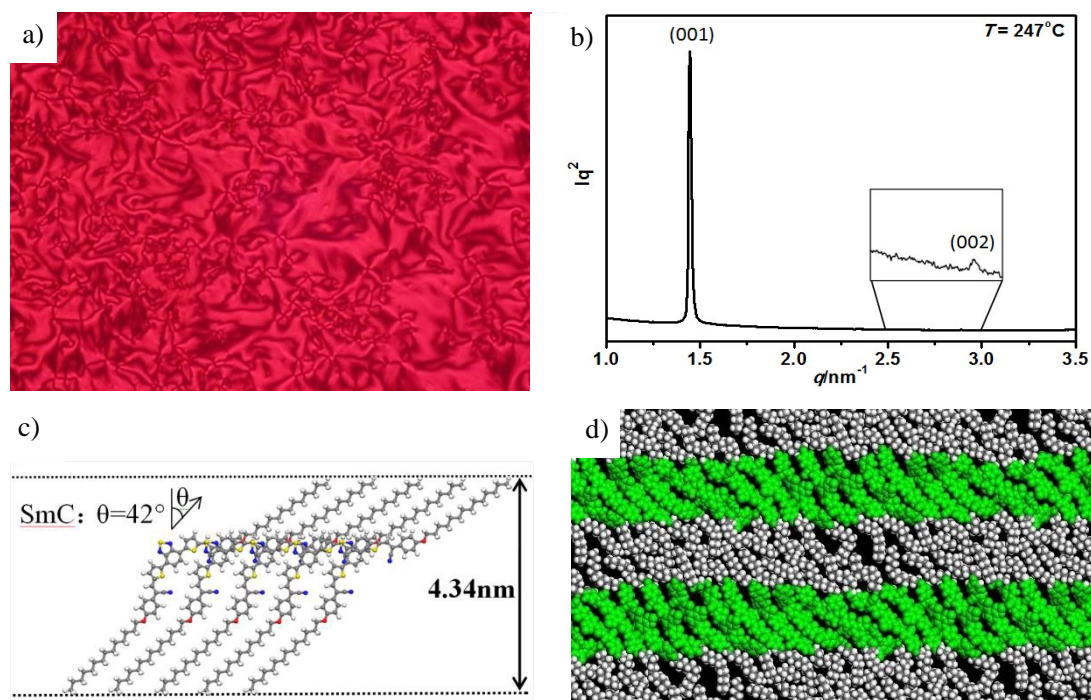


Fig. 1 SmC phase of compound **I¹/**14****: a) texture as seen between crossed polarizer at $T = 220$ °C cooling from isotropic state; b) SAXS pattern at $T = 247$ °C; c) the model of the molecular organization in monolayer of the SmC phase; d) snapshot after MD annealing.

2.2.2. Hexagonal columnar phase

The columnar phase of hexacatenar **I**³/**16** which showed spherulitic fan-like textures was characterized by the POM (Fig. S1e). The SAXS pattern of the columnar phase of **I**³/**16** (Fig. 2a) showed three small-angle reflection peaks at 4.70 (10), 2.72 (11), and 2.37 (20) nm with the reciprocal spacing ratio of 1 : 3^{1/2} : 2, indicating a hexagonal columnar (Col_{hex}) arrangement.¹⁹ The number of molecules (μ) in a slice of the columns with a height of $h = 0.45$ nm (maximum of the diffuse wide angle scattering) was calculated to be about three (Table 1). Thus three molecules self-assemble into a flat disc (Fig. 2c). In order to magnify the dipolar interactions, the central BTD dipole should point to the centre of the supramolecular disc. Then the discs further pile up into columns with 60° alternation along the columnar axis from one disc to the next. The space surrounding the column can be filled by the interlocking and folding of the alkyl chains.²⁰ The model of the hexagonal columnar phase was shown in Fig. 2c. It should be noted that the intermolecular π - π interactions, strong dipole-dipole interactions caused by the cyano, BTD, thiophene groups, as well as the microsegregation of the rigid aromatic core from the peripheral alkyl chains would drive the molecular assembly into the columnar structures. The length of the biscyanovinyl dithienebenzothiadiazole central unit is 3.15 nm, which is corresponding to the diameter of the regions of medium electron density (green) as shown in Fig. 2b. These diameters are also in good agreement with the sizes of the cores (green) and alkyl chains (off-white) in the molecular dynamics (MD) annealed model in Fig. 2d.^{21,22} The alkyl chains are completely disordered and partly interdigitated in the continuum of low electron density around these columns.

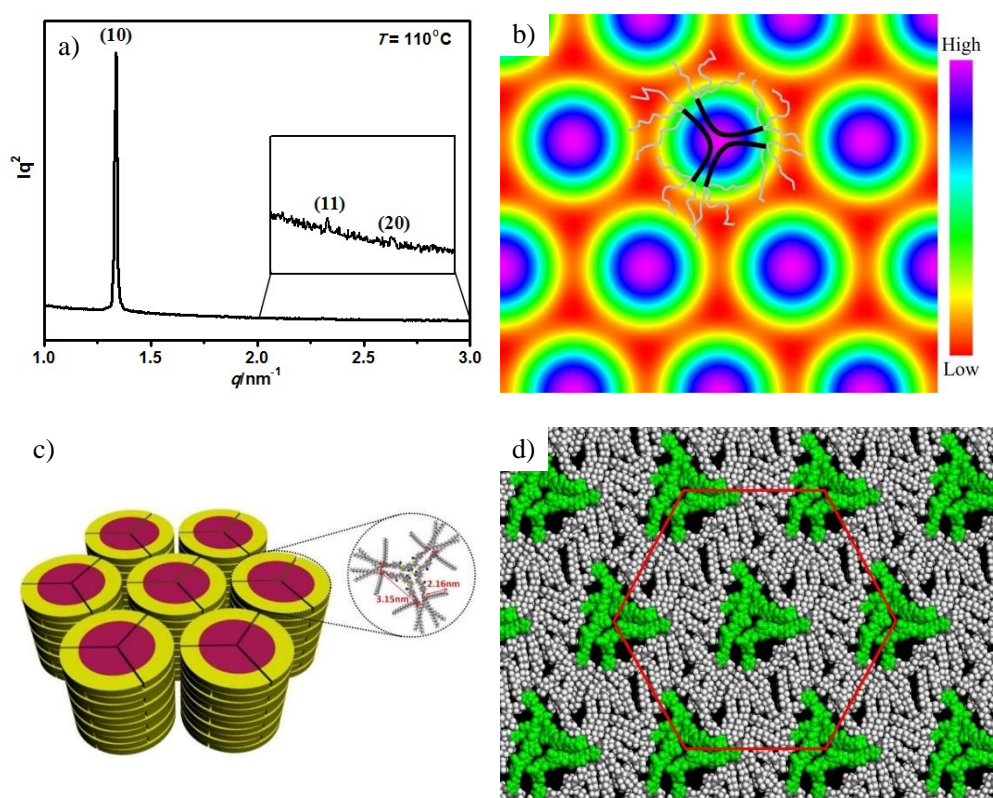


Fig. 2 Col_{hex} phase of compound **I**³/**16**: a) SAXS diffractogram at $T = 110$ °C; b) electron density map area constructed from the diffraction pattern in (a), and the color code was shown on the right; c) models for the molecular arrangement in Col_{hex}/*p6mm* phase; d) snapshots after MD annealing.

2.3. Gelation properties

The gelation abilities of compounds \mathbf{I}^m/n for different organic solvents were evaluated at the critical gelation concentration (CGC) of 4.0 mg mL^{-1} (Table 2). The relationship of the gel stability and T_{gel} (the temperature at which the gel is broken) indicated that the gel stability increased with increasing the gelator concentration (Fig. S5). The representative dicatenar compound $\mathbf{I}^1/16$ cannot form gel, while compound $\mathbf{I}^3/16$ can form gel in ethyl acetate: petroleum ether = 1 : 1. Blackred gel was formed in ethyl acetate : petroleum ether = 1 : 1 by cooling the heated solution of compound $\mathbf{I}^3/16$ to room temperature (Fig. 3a and Fig. S6). The morphology of the xerogel formed by $\mathbf{I}^3/16$ was investigated by scanning electron microscopy (SEM). Fig. 3b showed the formation of three-dimensional fibrous networks. The length of the fibers is more than $20 \mu\text{m}$ with a diameter of $0.27\text{-}1.35 \mu\text{m}$. It should be mentioned that there is no gelating functional groups such as amide, cholesterol, triazol and acetylene etc. in the structure of compound $\mathbf{I}^3/16$, therefore the gelation property of compound $\mathbf{I}^3/16$ in solution should be mainly promoted by donor-acceptor interaction, $\pi\text{-}\pi$ interactions and van der Waals forces.

Table 2 Gelation properties of compounds $\mathbf{I}^1/16$ and $\mathbf{I}^3/16$.^a

Solvent	$\mathbf{I}^1/16$	$\mathbf{I}^3/16$	Solvent	$\mathbf{I}^1/16$	$\mathbf{I}^3/16$
Chloroform	P	S	1,4-Dioxane	P	P
Ethyl acetate	P	IS	Hexane	P	IS
THF	S	S	Toluene	P	S
Ethanol	P	P	Dichloromethane	P	S
Acetone	P	P	Ethyl acetate : petroleum ether =1:1	P	G
Petroleum ether	P	S			

^aS = solution, P = precipitation, G = gelation, IS = insoluble gelator.

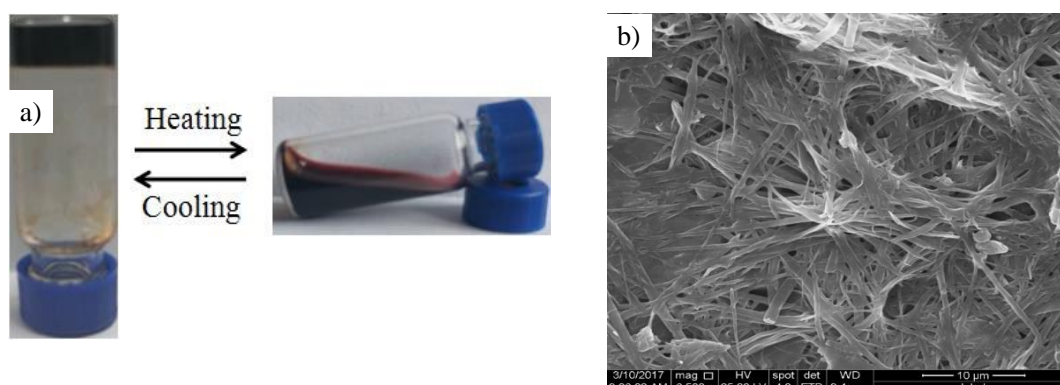


Fig. 3 a) Photos of gel prepared with compound $\mathbf{I}^3/16$ in ethyl acetate : petroleum ether = 1 : 1 at $20 \text{ }^\circ\text{C}$; b) SEM image of xerogel formed by compound $\mathbf{I}^3/16$.

2.4. Absorption and emission properties

The UV-vis absorption and emission spectra of two representative compounds $\mathbf{I}^1/16$ and $\mathbf{I}^3/16$ in

DCM are shown in Fig. 4. Compounds **I¹/16** and **I³/16** exhibited dual-band absorptions in the ranges of 330-440 nm and 440-625 nm, corresponding to the π - π^* transition and internal charge transfer (ICT) transition between the donor and acceptor units respectively.^{14d,23} The emission bands are in the ranges of 632 nm to 653 nm, therefore the Stokes shifts are 111-136 nm. The absorption and emission spectra of **I¹/16** and **I³/16** have similar shape, indicating that the electronic properties of both compounds are dictated by the similar extended chromophore. The absorption edge of **I¹/16** is red shifted slightly compared to that of **I³/16**, which indicates that the terminal alkoxy substituent in **I¹/16** is a better donor than the benzyloxy moiety in **I³/16**.

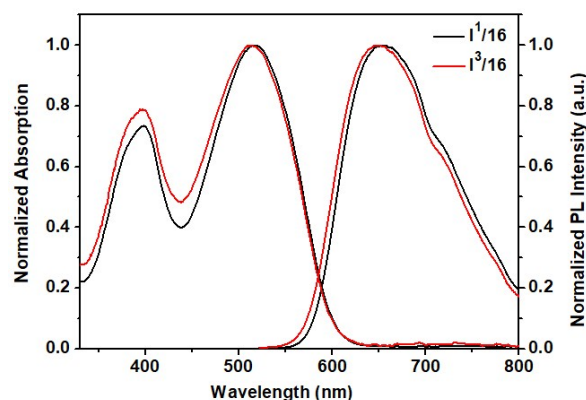


Fig. 4 Normalized UV-vis absorption and emission spectra of compounds **I¹/16** and **I³/16** (10^{-6} M) at 20 °C in DCM.

The solvatochromic behaviors of compounds **I^m/n** were investigated in organic solvents with different polarity from toluene to THF (shown in Fig. S7) and the photophysical data were listed in Table S7. As shown in Fig. S7g, the solvent polarity has less impact on the absorption spectra of **I¹/16**, which exhibits two prominent bands at $\lambda = 330$ -440 nm and $\lambda = 440$ -625 nm. The fluorescence spectra (Fig. S7h) however, showed evidently solvatochromism (red-shifted from 632 nm in toluene to 653 nm in THF) as the polarity of solvents increased. Therefore **I^m/n** have large Stokes shifts (111-136 nm). The wavelength range of compounds **I^m/n** are close to near infrared and wider than those of the literatures reported biscyanovinyl dithienebenzothiadiazole analogues.^{24,25,26} The ICT effect should cause the solvatochromism in fluorescence. Because ICT compounds usually have large dipole moments in the excited state, therefore the dipole-dipole interactions between polar solvent and ICT compounds would reduce the energy of the excited state.²⁷

The energy band gaps of compounds **I¹/16** and **I³/16** can be estimated from the UV spectra of the thin film to be about 1.79 eV (Fig. S8).²⁸ Using Gaussian 09 software, by density functional theory (DFT) based on B3LYP with a polarized 6-31G(d) basis,²⁹ the ground-state geometries and electronic structures of **I¹/16** and **I³/16** were calculated. The electron distributions of the HOMO and LUMO of **I¹/16** and **I³/16**, in which the alkoxy chains are replaced by methoxy groups, are shown in Fig. S9. The calculation results show that the central dithienebenzothiadiazole moiety with its two adjacent cyanovinyl 4-alkoxyphenyl units, represents a large conjugated planar conformation. While the structure of **I³/16** appears a slightly non-planar from the methylene connected on the terminal alkoxyphenyl moieties. In these two compounds, electron density of the HOMO localized on the rigid π -conjugated dithienebenzothiadiazole and cyanovinyl 4-alkoxyphenyl units. In the LUMO orbital however the electrons are localized on the central of

dithienbenzothiadiazole unit. It indicates that during the molecule excited from HOMO to LUMO energy levels, a charge transfers from the alkoxyphenyl units to the central dithienbenzothiadiazole moiety might be occurred. Such photophysical properties indicated that these molecules could be applied in fabrication of high performance solution processable photoelectrical molecular devices such as OPV and OLEDs.

It was found that the fluorescence emission of **I¹/16** could be significantly quenched as the concentration of C₇₀ increased (Fig. 5 and Fig. S10). This phenomenon indicated the presence of photoinduced charge separation process between **I¹/16** and C₇₀.³⁰ To further study the quenching constant (K_{SV}) of C₇₀ to **I¹/16**, the dependence of fluorescence intensity on the concentration of C₇₀ at low quencher concentrations was analyzed. It agreed with the Sterne-Volmer equation.

$$F_0/F = 1 + K_{SV} \cdot C$$

Here, F_0 and F represent the fluorescence intensity in the absence and present of C₇₀, respectively, and C is the concentration of C₇₀. The K_{SV} value of **I¹/16** is $1.7 \times 10^4 \text{ M}^{-1}$.

The charge separation led to photoinduced electron transfer. Therefore there could exist electron transfer between BTD fluorophore and C₇₀,³¹ this indicated that the BTD fluorophore–fullerene blend was favorable component for fabrication the highly efficient photovoltaic (PV) cells.

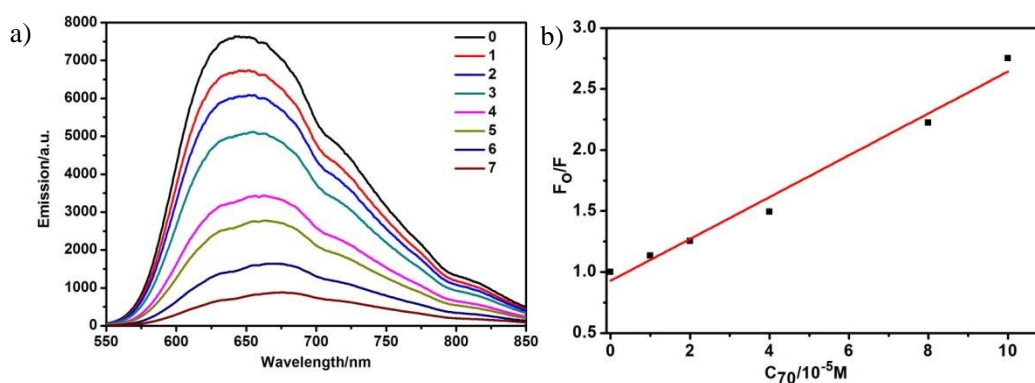


Fig. 5 a) Emission spectra (left) of **I¹/16** ($1.0 \times 10^{-5} \text{ M}$) in CHCl_3 with increasing concentration of C₇₀ ($1.0 \times 10^{-5} \text{ M}$): 0.0 (0), 1.0 (1), 2.0 (2), 4.0 (3), 8.0 (4), 10.0 (5); b) Sterne-Volmer quenching plots for **I¹/16**.

2.5. Optical waveguide behavior

The compounds **I¹/n** ($n = 10, 12, 14, 16, 18$) can form needle crystals in DCM/MeOH and cubic crystals in THF/petroleum ether (Fig. 6 and Fig. S11). For compound **I¹/18**, the needle aggregates are about 1.7-6.7 μm in width and 128-267 μm in length (Fig. S11i), whereas the cubic aggregates are about 3.7-10 μm in width (Fig. S11j). These aggregates were investigated by the fluorescent microscope. Irradiated with a light beam at different λ , these aggregates exhibited very bright red luminescence at both sides but relatively weaker emission from the body. It suggested that these compounds exhibited optical waveguide behavior.³² It showed that these solvated crystals could be used as light-emitting and propagation materials in miniaturized optoelectronic devices.



Fig. 6 Photoluminescence microscopy images of the crystalline aggregates at 540-560 nm of **I¹/12** produced in THF/petroleum ether mixed solution.

2.6. Chemosensor behavior

The selective binding abilities of compounds **I^m/n** towards different metal ions (all anions are ClO_4^-), including Ag^+ , Cd^{2+} , Co^{2+} , Cu^{2+} , Hg^{2+} , K^+ , Li^+ , Mg^{2+} , Ni^+ , Pb^{2+} , Zn^{2+} , Cr^{3+} , Fe^{3+} and Al^{3+} , were examined. The concentration of all metal ions is $10^{-3} \text{ mol L}^{-1}$. All compounds **I^m/n** can recognize Cu^{2+} . The result of the representative compound **I¹/10** was shown in Fig. 7. The fluorescence spectra of **I¹/10** by the addition of 20 equiv. of selected cations in $\text{CH}_3\text{CN} : \text{DCM} = 2 : 1$ solution were investigated. No obvious change of the fluorescence intensity of the compound **I¹/10** by addition of most metal ions. Only upon the increasing addition of Cu^{2+} (Fig. 7a and Fig. S12a), obvious fluorescence quenching was observed. The selective response of **I¹/10** to Cu^{2+} can be detected by naked eye as shown in Fig. 7b. The selective response of **I¹/10** to Cu^{2+} was examined by fluorescence titration with addition of Cu^{2+} (from 0 to 25 equiv.) in solution of $\text{CH}_3\text{CN} : \text{DCM} = 2 : 1$. It was clearly shown that the fluorescence reached its quenching plateau by addition of about 16 equiv. of Cu^{2+} (Fig. S12b, c).³³ The calculated detection limit of **I¹/10** towards Cu^{2+} was $4.83 \times 10^{-7} \text{ M}$ based on $3\sigma/k$ ³⁴ (Fig. S13), which is much lower than those of the reported α -cyanostilbene-based chemosensors.³⁵ Therefore, compound **I¹/10** could be used as Cu^{2+} chemosensor with high selectivity and low detection limit in the solution of $\text{CH}_3\text{CN} : \text{DCM} = 2 : 1$. The binding stoichiometry was determined by Job's plot method, indicating that compound **I¹/10** and Cu^{2+} could form a 1 : 1 complex (Fig. S14). The FTIR spectrum of **I¹/10** (Fig. S15a) indicated that the characteristic peak at 2310 cm^{-1} was assigned to the $\text{C}\equiv\text{N}$ stretching vibration.³⁶ After interacting with Cu^{2+} , the peak of $\text{C}\equiv\text{N}$ stretching vibration showed obvious blue shift to 2248 cm^{-1} . It indicated that the N atom of $\text{C}\equiv\text{N}$ of compound **I¹/10** was the binding site. This indicated that the coordination of Cu^{2+} with $\text{C}\equiv\text{N}$ induced fluorescence quenching of **I^m/n** solutions. Therefore the chelation enhanced quenching (CEQ) sensing mechanism³⁷ was the main reason for inducing fluorescence quenching of **I^m/n** solutions. In the FTIR spectra of **I¹/10**+other metal ions, the characteristic peaks at 2310 cm^{-1} showed little change (Fig. S15b) indicating no binding interaction between **I^m/n** and other metal ions. It should be noted that even though BTDA α -cyanostilbene derivatives could display excellent fluorescence property,^{12a,12b,13,38,39} however their application as fluorescent probe are few. Therefore, this should be the first time that the chemosensor behaviors of such compounds have been studied. The aggregation-induced emission (AIE) of biscyanovinyl dithienebenzothiadiazole has not been observed, probably ascribed to the

strong fluorescence properties of BTD.

View Article Online
DOI: 10.1039/C8NJ02814A

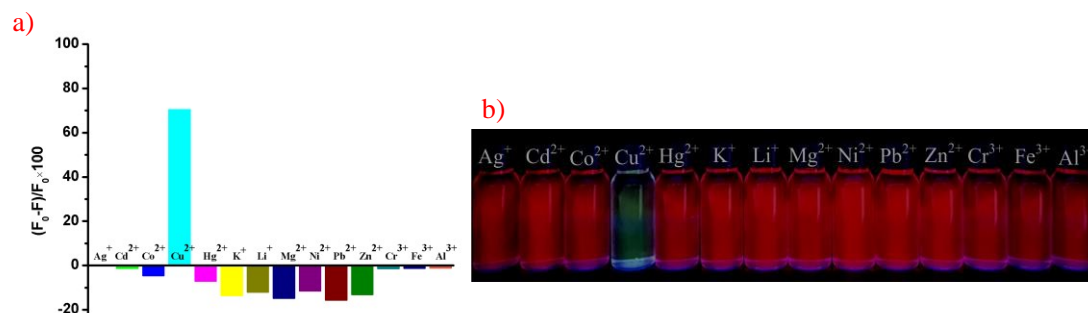


Fig. 7 The fluorescence response of **I¹/10** (10^{-6} M, $\text{CH}_3\text{CN} : \text{DCM} = 2 : 1$) upon addition of different metal ions (20 equiv.) at $\text{pH} = 7.0$ (a and b) ($\lambda_{\text{ex}} = 510$ nm); F_0 = the fluorescence emission maximum of a blank sample; F = the fluorescence emission maximum of samples with addition of different metal ions; b) Fluorescence changes of **I¹/10** (10^{-6} M) on addition of different metal ions (20 equiv.).

3. Conclusions

In conclusion, D-A fluorophores based on cyanovinyl and BTD have been successfully synthesized. The liquid crystalline properties of these fluorophores were well investigated by POM, DSC and XRD. They can self-assemble into SmC and $\text{Col}_{\text{hex}}/p6mm$ phases. Suggested phase structures are based on XRD patterns, electron density reconstruction and simulations. The molecular packing models for these phase structures are well established. Additionally the compound **I³/16** can also self-assemble into organogel in solvents. These fluorophores exhibit broad and strong absorption band at the range of 330-625 nm with a red emissive color and large Stokes shifts. The fluorescence emission of the compound **I¹/16** in CHCl_3 was significantly quenched upon addition of C_{70} , indicating the presence of electron transfer between BTD compounds and C_{70} . In organic solvents, these red emissive molecules can form solvated crystals, which exhibit optical waveguide behaviors. Finally these compounds can act as chemosensors for detection of Cu^{2+} . Thus, these multifunctional materials can be potentially applied in diverse areas such as liquid crystals, chemosensors, red emission waveguides etc.

Acknowledgment

We thank National Natural Science Foundation of China (Nos. 21664015 and 21602195) and the Yunnan Science Foundation (No. 201701UH00095) for financial supports. We thank beamline BL16B1 at Shanghai Synchrotron Radiation Facility (SSRF), China. The calculations were performed with the support of the Yunnan University Supercomputer Center.

References

- [a] K. Müllen and G. Wegner, *Electronic materials, the oligomer approach*, Wiley-VCH, Weinheim, Germany, 1998; [b] G. Yu, J. Gao, J. C. Hummelen, F. Wudl and A.J. Heeger, *Science*, 1995, **270**, 1789-1791; [c] S. Günes,

- H. Neugebauer and N. S. Sariciftci, *Chem. Rev.*, 2007, **107**, 1324-1338; [d] J. Y. Kim, K. Lee, N. E. Coates, D. Moses, T. Q. Nguyen and M. Dante, *Science*, 2007, **317**, 222-225; [e] Y. Liang, Y. Wu, D. Feng, S. T. Tsai, H. J. Son and G. Li, *J. Am. Chem. Soc.*, 2009, **131**, 56-57.
- 2 [a] T. Nishizawa, H. K. Lim, K. Tajima and K. Hashimoto, *Chem. Commun.*, 2009, **18**, 2469-2471; [b] L. Schmida-Mende, A. Fechtenkotter, K. Müllen, E. Moons, R. H. Friend and J. D. Mackenzie, *Science*, 2001, **293**, 1119-1122; [c] J. Pei, J. L. Wang, X. Y. Cao, X. H. Zhou and W. B. Zhang, *J. Am. Chem. Soc.*, 2003, **125**, 9944-9945; [d] M. T. Lloyd, A. C. Mayer, S. Subramanian, D. A. Mourney, D. J. Herman and A. Bapat, *J. Am. Chem. Soc.*, 2007, **129**, 9144-9149; [g] C. Q. Ma, E. Mena-Osteritz, T. Debaerdemaeker, M. M. Wienk, R. A. J. Janssen and P. Bäuerle, *Angew. Chem. Int. Ed.*, 2007, **46**, 1679-1683; [e] C. Q. Ma, E. Mena-Osteritz, T. Debaerdemaeker, M. M. Wienk, R. A. J. Janssen and P. Bäuerle, *Angew. Chem. Int. Ed.*, 2007, **46**, 1679-1683.3
- D. Demus, J. W. Goodby, G. W. Gray, H.W. Spiess and V. Vill, *Handbook of liquid crystal*, VCH-Wiley, Weinheim, 1998.
- 4 J. J. M. Halls, C. A. Walsh, N. C. Greenham, E. A. Marseglla, R. H. Friend and S. C. Moratti, *Nature*, 1995, **376**, 498-500.
- 5 [a] L. L. Zhu and Y. L. Zhao, *J. Mater. Chem. C*, 2013, **1**, 1059-1065; [b] M. Martínez-Abadía, R. Giménez and M. B. Ros, *Adv. Mater.*, 2017, **170**, 41-61.
- 6 [a] N. Blouin, A. Michaud, D. Gendron, S. Wakim, E. Blair and R. Neagu-Plesu, *J. Am. Chem. Soc.*, 2008, **130**, 732-742; [b] M. Melucci, L. Favaretto, A. Zanelli, M. Cavallini, A. Bongini and P. Maccagnani, *Adv. Funct. Mater.*, 2010, **20**, 445-452; [c] W. Zhu, X. Meng, Y. Yang, Q. Zhang, Y. Xie and H. Tian, *Chem. Eur. J.*, 2010, **16**, 899- 906. [d] Q. Zou and H. Tian, *Sens. Actuators B*, 2010, **149**, 20-27; [e] P. Beaujuge, W. Pisula, H. N. Tsao, S Ellinger, K Müllen and J. R. Reynolds, *J. Am. Chem. Soc.*, 2009, **131**, 7514-7515.
- 7 [a] P. Beaujuge, W. Pisula, H. N. Tsao, S Ellinger, K Müllen and J. R. Reynolds, *J. Am. Chem. Soc.*, 2009, **131**, 7514-7515; [b] W. Li, C. Du, F. Li, Y. Zhou, M. Fahlman and Z. Bo, *Chem. Mater.*, 2009, **21**, 5327-5334; [c] Y. Li, A. Y. Li, B. X. Li, J. Huang, L. Zhao and B. Z. Wang, *Org. Lett.*, 2009, **11**, 5318-5321; [d] L. Huo, J. Hou, S. Zhang, H. Y. Chen and Y. Yang, *Angew. Chem. Int. Ed.*, 2010, **49**, 1500-1503.
- 8 Y. Yang, Y. Zhou, Q. He, C. He, C. Yang and F. Bai, *J. Phys. Chem. B*, 2009, **113**, 7745-7752.
- 9 D. X. Huang, M. Prehm, H. F. Gao, X. H. Cheng, Y. S. Liu and C. Tschierske, *RSC Adv.*, 2016, **6**, 21387-21395.
- 10 P. F. Xia, J. Lu, C. H. Kwok, H. Fukutani, M. S. Wong and Y. Tao, *J. Polym. Sci. Part A: Polym. Chem.*, 2008, **47**, 137-48.
- 11 B. A. D. Neto, A. A. M. Lapis and S. Júnior, *Eur. J. Org. Chem.*, 2013, **12**, 228-255.
- 12 [a] S. Zeng, L. Yin, C. Ji, X. Jiang, K. Li and Y. Li, *Chem. Commun.*, 2012, **48**, 10627-10629. [b] P. Suresh, P. Balraju, G. D. Sharma, J. A. Mikroyannidis and M. M. Stylianakis, *ACS Appl. Mater. Interfaces.*, 2009, **1**, 1370-1374; [c] G. D. Sharma, P. Balraju, J. A. Mikroyannidis and M. M. Stylianakis, *Sol. Energy Mater. Sol. Cells*, 2009, **93**, 2025-2028; [d] J. A. Mikroyannidis, M. M. Stylianakis, Q. Dong, J. Pei and W. Tian, *J. Appl. Polym. Sci.*, 2009, **114**, 2740-2750.
- 13 C. Chen, D. H. Maldonado, D. L. Borgne, F. Alary, B. Lonetti and B. Heinrich, *New J. Chem.*, 2016, **40**, 7326-7337.
- 14 [a] W. Ni, X. J. Wan, M. M. Li, Y. C. Wang and Y. S. Chen, *Chem. Commun.*, 2015, **51**, 4936-4950; [b] Y. Chen, X. Wan and G. Long, *Acc. Chem. Res.*, 2013, **46**, 2645-2655; [c] J. L. Wang, Q. Xiao and J. Pei, *Org. Lett.*, 2010, **12**, 4164-4167; [d] X. Z. Li, A. H. Liu, S. D. Xun, W. Q. Qiao, X. H. Wan and Z. Y. Wang, *Org. Lett.*, 2008, **10**, 3785-3787.
- 15 [a] M. Müri, K. C. Schuermann, L. D. Cola and M. Mayor, *Eur. J. Org. Chem.*, 2009, **15**, 2562-2575; [b] M. Yoshio, T. Kagata, K. Hoshino, T. Mukai, H. Ohno and T. Kato, *J. Am. Chem. Soc.*, 2006, **128**, 5570-5577; [c] X. H. Cheng, X. Bai, S. Jing, H. Ebert, M. Prehm and C. Tschierske, *Chem. Eur. J.*, 2010, **16**, 4588-4601; [d] S.

- H. Seo, J. H. Park, G. N. Tew and J. Y. Chang, *Tetrahedron Lett.*, 2007, **48**, 6839-6844.
- 16 I. Dierking, *Textures of liquid crystals*, 2003.
- 17 [a] Ch. CAe, Oxford Molecular Ltd, Oxford, UK, 1999; [b] Identical values were obtained with CPK models.
- 18 H. Cai, B. Gabryelczyk, M. S. S. Manimekalai, G. Grüber, S. Salentinig and A. Miserez, *Soft Matter*, 2017, **13**, 7740-7752.
- 19 X. Peng, H. Gao, Y. Xiao, H. Cheng, F. Huang and X. Cheng, *New J. Chem.*, 2017, **41**, 2004-2012.
- 20 [a] E. Goreck, D. Pocięcha, J. Mieczkowski, J. Matraszek, D. Guillon and B. Donnio, *J. Am. Chem. Soc.*, 2004, **126**, 15946-15947; [b] A. Lesac, B. Donnio and D. Guillon, *Soft Matter*, 2009, **5**, 4231-4239.
- 21 M. Prehm, F. Liu, U. Baumeister, X. Zeng, G. Ungar and C. Tschierske, *Angew. Chem. Int. Ed.*, 2007, **46**, 7972-7975.
- 22 H. J. Kim, F. Liu, J. H. Ryu, S. K. Kang, X. Zeng and G. Ungar, *J. Am. Chem. Soc.*, 2012, **134**, 13871-13880.
- 23 [a] C. F. Huang, J. Y. Chang, S. H. Huang, K. Y. Wu, J. F. Jheng and W. T. Chuang, *J. Mater. Chem. A*, 2015, **3**, 3968-3974; [b] G. Zhang, J. Chen, Y. Dai, S. Song, Z. Ye and H. Lu, *Dyes. Pigm.*, 2017, **137**, 221-228.
- 24 C. Chen, D. H. Maldonado, D. L. Borgne, F. Alary, B. Lonetti and B. Heinrich, *New J. Chem.*, 2016, **40**, 7326-7337.
- 25 J. A. Mikroyannidis, M. M. Stylianakis, Q. Dong, Y. Zhou and W. Tian, *Synth. Met.*, 2009, **159**, 1471-1477.
- 26 J. A. Mikroyannidis, M. M. Stylianakis, P. Suresh, P. Balraju and G. D. Sharma, *Org. Electron.*, 2009, **10**, 1320-1333.
- 27 S. Grimme, C. Diedrich and M. Korth, *Angew. Chem. Int. Ed.*, 2006, **45**, 625-629.
- 28 [a] R. S. Dariani and R. Zafari, *J. Optoelectron Adv. M.*, 2014, **16**, 1351-1355; [b] M. Hamaguchi, H. Sawada, J. Kyokane and K. Yoshino, *Chem. Lett.*, 1996, **7**, 527-528.
- 29 M. J. Frisch, G. W. Trucks, H. B. Schlegel, G. E. Scuseria, M. A. Robb and J. R. Cheeseman, Gaussian 09, revision A1. Wallingford CT: Gaussian, 2009.
- 30 [a] S. Zeng, L. Yin, X. Jiang, Y. Li and K. Li, *Dyes. Pigm.*, 2012, **95**, 229-235. [b] B. K. Ghosh, A. Bauri, S. Bhattacharya and S. Banerjee, *Spectrochim Acta A*, 2014, **125**, 90-98.
- 31 T. Zhang, H. Han, Y. Zou, Y. C. Lee, H. Oshima, K. T. Wong, *ACS Appl. Mater. Interfaces*, 2017, **9**, 25418-25425.
- 32 [a] S. Chen, N. Chen, Y. L. Yan, T. Liu, Y. Yu and Y. Li, *Chem. Commun.*, 2012, **48**, 9011-9013; [b] K. Balakrishnan, A. S. Sayyad, G. Myhre, S. Mataka and S. Pau, *Chem. Commun.*, 2012, **48**, 11668-11670; [c] X. Gu, J. Yao, G. Zhang, Y. Yan, C. Zhang and Q. Peng, *Adv. Funct. Mater.*, 2012, **22**, 4862-4872; [d] L. Heng, X. Wang, D. Tian, J. Zhai, B. Tang and L. Jiang, *Adv. Mater.*, 2010, **22**, 4716-4720; [e] E. Wang, J. W. Y. Lam, R. Hu, C. Zhang, Y. S. Zhao and B. Z. Tang, *J. Mater. Chem C.*, 2014, **2**, 1801-1807.
- 33 X. P. He, Z. Song, Z. Z. Wang, X. X. Shi, K. Chen and G. R. Chen, *Tetrahedron*, 2011, **67**, 3343-3347.
- 34 I. J. Kim, R. Manivannan and Y. A. Son, *Sens. Actuators B*, 2017, **246**, 319-326.
- 35 T. Ghosh, A. Vyas, K. Bhayani and S. Mishra, *J. Fluoresc.*, 2018, **11**, 1-10.
- 36 [a] J. Mitra, M. Saxena, N. Paul, E. Saha, R. Sarkar and S. Sarkar, *New J. Chem.*, 2018, **42**, 14229-14238; [b] S. K. Moosvia, K. Majida and T. Araa, *Materials Research*, 2016, **19**, 983-990.
- 37 A.W. Czarnik, *Fluorescent Chemosensors for Ion and Molecule Recognition*, American Chemical Society, Washington DC, 1992.
- 38 C. D. Dou, D. Chen, J. Iqbal, Y. Yuan, H. Y. Zhang and Y. Wang, *Langmuir*, 2011, **27**, 6323-6329.
- 39 H. T. Zhou, W. Huang, L. Ding, S. Y. Cai, X. Li, B. Li and J. H. Su, *Tetrahedron*, 2014, **70**, 7050-7056.

Graphical abstracts

Mesogenic D-A fluorophores based on cyanovinyl and benzothiadiazole

Bei Zhang,^{‡[a]} Yulong Xiao,^{‡[a]} Haipeng Fang,^[a] Hongfei Gao,^[a] Fuke Wang,^{*[b]}
Xiaohong Cheng^{*[a]}

[a] Key Laboratory of Medicinal Chemistry for Natural Resources, Chemistry Department,
Yunnan University
Kunming,
Yunnan 650091,
P. R. China
Fax: (+86) 871 65032905
E-mail: xhcheng@ynu.edu.cn

[b] Department of Sports Medicine, First Affiliated Hospital of Kunming Medical University
E-mail: wfk.04@126.com

[‡]Both authors contributed equally to this work

